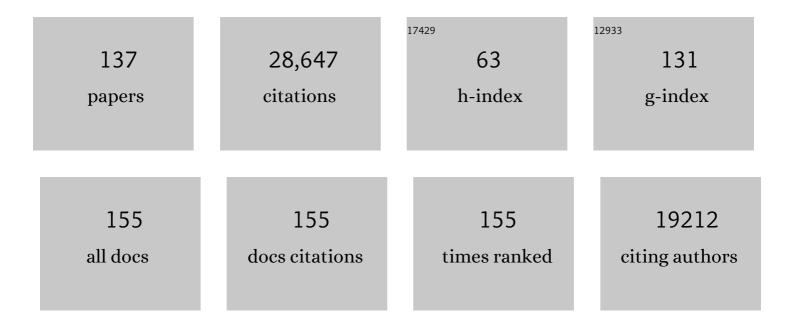
List of Publications by Year in descending order

Source: https://exaly.com/author-pdf/11766782/publications.pdf Version: 2024-02-01



FSSA VACOUR

#	Article	lF	CITATIONS
1	The WU-Minn Human Connectome Project: An overview. NeuroImage, 2013, 80, 62-79.	2.1	4,282
2	A multi-modal parcellation of human cerebral cortex. Nature, 2016, 536, 171-178.	13.7	3,634
3	Multimodal population brain imaging in the UK Biobank prospective epidemiological study. Nature Neuroscience, 2016, 19, 1523-1536.	7.1	1,414
4	Resting-state fMRI in the Human Connectome Project. NeuroImage, 2013, 80, 144-168.	2.1	1,367
5	Multiband multislice GEâ€EPI at 7 tesla, with 16â€fold acceleration using partial parallel imaging with application to high spatial and temporal wholeâ€brain fMRI. Magnetic Resonance in Medicine, 2010, 63, 1144-1153.	1.9	1,329
6	Multiplexed Echo Planar Imaging for Sub-Second Whole Brain FMRI and Fast Diffusion Imaging. PLoS ONE, 2010, 5, e15710.	1.1	1,164
7	ICA-based artefact removal and accelerated fMRI acquisition for improved resting state network imaging. NeuroImage, 2014, 95, 232-247.	2.1	1,148
8	Advances in diffusion MRI acquisition and processing in the Human Connectome Project. NeuroImage, 2013, 80, 125-143.	2.1	851
9	The Human Connectome Project's neuroimaging approach. Nature Neuroscience, 2016, 19, 1175-1187.	7.1	825
10	Pushing spatial and temporal resolution for functional and diffusion MRI in the Human Connectome Project. NeuroImage, 2013, 80, 80-104.	2.1	769
11	Sustained Negative BOLD, Blood Flow and Oxygen Consumption Response and Its Coupling to the Positive Response in the Human Brain. Neuron, 2002, 36, 1195-1210.	3.8	565
12	High-field fMRI unveils orientation columns in humans. Proceedings of the National Academy of Sciences of the United States of America, 2008, 105, 10607-10612.	3.3	500
13	Evaluation of slice accelerations using multiband echo planar imaging at 3T. NeuroImage, 2013, 83, 991-1001.	2.1	442
14	Imaging brain function in humans at 7 Tesla. Magnetic Resonance in Medicine, 2001, 45, 588-594.	1.9	421
15	Microvascular BOLD contribution at 4 and 7 T in the human brain: Gradient-echo and spin-echo fMRI with suppression of blood effects. Magnetic Resonance in Medicine, 2003, 49, 1019-1027.	1.9	331
16	Reconstruction of the orientation distribution function in single―and multipleâ€shell qâ€ball imaging within constant solid angle. Magnetic Resonance in Medicine, 2010, 64, 554-566.	1.9	329
17	Contextual Feedback to Superficial Layers of V1. Current Biology, 2015, 25, 2690-2695.	1.8	303
18	Extending the Human Connectome Project across ages: Imaging protocols for the Lifespan Development and Aging projects. NeuroImage, 2018, 183, 972-984.	2.1	290

#	Article	IF	CITATIONS
19	Spin-echo fMRI in humans using high spatial resolutions and high magnetic fields. Magnetic Resonance in Medicine, 2003, 49, 655-664.	1.9	284
20	Spatio-temporal point-spread function of fMRI signal in human gray matter at 7 Tesla. NeuroImage, 2007, 35, 539-552.	2.1	266
21	T1 weighted brain images at 7ÂTesla unbiased for Proton Density, T2⎠contrast and RF coil receive B1 sensitivity with simultaneous vessel visualization. NeuroImage, 2009, 46, 432-446.	2.1	260
22	Robust detection of ocular dominance columns in humans using Hahn Spin Echo BOLD functional MRI at 7 Tesla. NeuroImage, 2007, 37, 1161-1177.	2.1	258
23	The UNC/UMN Baby Connectome Project (BCP): An overview of the study design and protocol development. NeuroImage, 2019, 185, 891-905.	2.1	234
24	Heritability of fractional anisotropy in human white matter: A comparison of Human Connectome Project and ENIGMA-DTI data. NeuroImage, 2015, 111, 300-311.	2.1	227
25	Ultrahigh field magnetic resonance imaging and spectroscopy. Magnetic Resonance Imaging, 2003, 21, 1263-1281.	1.0	218
26	An Assessment of Current Brain Targets for Deep Brain Stimulation Surgery With Susceptibility-Weighted Imaging at 7 Tesla. Neurosurgery, 2010, 67, 1745-1756.	0.6	202
27	An Open Resource for Non-human Primate Imaging. Neuron, 2018, 100, 61-74.e2.	3.8	190
28	Encoding of Natural Sounds at Multiple Spectral and Temporal Resolutions in the Human Auditory Cortex. PLoS Computational Biology, 2014, 10, e1003412.	1.5	187
29	The Lifespan Human Connectome Project in Aging: An overview. NeuroImage, 2019, 185, 335-348.	2.1	186
30	The Lifespan Human Connectome Project in Development: A large-scale study of brain connectivity development in 5–21 year olds. NeuroImage, 2018, 183, 456-468.	2.1	184
31	Signal and noise characteristics of Hahn SE and GE BOLD fMRI at 7 T in humans. NeuroImage, 2005, 24, 738-750.	2.1	182
32	Layer-Specific fMRI Reflects Different Neuronal Computations at Different Depths in Human V1. PLoS ONE, 2012, 7, e32536.	1.1	172
33	Evaluation of 2D multiband EPI imaging for high-resolution, whole-brain, task-based fMRI studies at 3T: Sensitivity and slice leakage artifacts. NeuroImage, 2016, 124, 32-42.	2.1	170
34	Combined imaging–histological study of cortical laminar specificity of fMRI signals. NeuroImage, 2006, 29, 879-887.	2.1	163
35	Mapping the Organization of Axis of Motion Selective Features in Human Area MT Using High-Field fMRI. PLoS ONE, 2011, 6, e28716.	1.1	163
36	Comprehensive in vivo Mapping of the Human Basal Ganglia and Thalamic Connectome in Individuals Using 7T MRI. PLoS ONE, 2012, 7, e29153.	1.1	159

#	Article	IF	CITATIONS
37	Frequency preference and attention effects across cortical depths in the human primary auditory cortex. Proceedings of the National Academy of Sciences of the United States of America, 2015, 112, 16036-16041.	3.3	153
38	Cortical Depth Dependent Functional Responses in Humans at 7T: Improved Specificity with 3D GRASE. PLoS ONE, 2013, 8, e60514.	1.1	151
39	High-resolution, spin-echo BOLD, and CBF fMRI at 4 and 7 T. Magnetic Resonance in Medicine, 2002, 48, 589-593.	1.9	145
40	The Human Connectome Project 7 Tesla retinotopy dataset: Description and population receptive field analysis. Journal of Vision, 2018, 18, 23.	0.1	139
41	Zoomed Functional Imaging in the Human Brain at 7 Tesla with Simultaneous High Spatial and High Temporal Resolution. NeuroImage, 2002, 17, 272-286.	2.1	134
42	A Hough transform global probabilistic approach to multiple-subject diffusion MRI tractography. Medical Image Analysis, 2011, 15, 414-425.	7.0	126
43	Multiband accelerated spinâ€echo echo planar imaging with reduced peak RF power using timeâ€shifted RF pulses. Magnetic Resonance in Medicine, 2013, 69, 1261-1267.	1.9	126
44	Perfusion-based high-resolution functional imaging in the human brain at 7 Tesla. Magnetic Resonance in Medicine, 2002, 47, 903-911.	1.9	117
45	Tradeoffs in pushing the spatial resolution of fMRI for the 7T Human Connectome Project. NeuroImage, 2017, 154, 23-32.	2.1	117
46	The Human Connectome Project: A retrospective. NeuroImage, 2021, 244, 118543.	2.1	114
47	The rapid development of high speed, resolution and precision in fMRI. NeuroImage, 2012, 62, 720-725.	2.1	109
48	Investigation of the initial dip in fMRI at 7 Tesla. NMR in Biomedicine, 2001, 14, 408-412.	1.6	108
49	Design of an MRI-Compatible Robotic Stereotactic Device for Minimally Invasive Interventions in the Breastâ€. Journal of Biomechanical Engineering, 2004, 126, 458-465.	0.6	107
50	The Evaluation of Preprocessing Choices in Single-Subject BOLD fMRI Using NPAIRS Performance Metrics. NeuroImage, 2003, 18, 10-27.	2.1	105
51	Mechanisms underlying decoding at 7ÂT: Ocular dominance columns, broad structures, and macroscopic blood vessels in V1 convey information on the stimulated eye. NeuroImage, 2010, 49, 1957-1964.	2.1	105
52	The Spatial Dependence of the Poststimulus Undershoot as Revealed by High-Resolution BOLD- and CBV-Weighted fMRI. Journal of Cerebral Blood Flow and Metabolism, 2006, 26, 634-644.	2.4	93
53	The impact of ultra-high field MRI on cognitive and computational neuroimaging. NeuroImage, 2018, 168, 366-382.	2.1	93
54	Accelerating the Evolution of Nonhuman Primate Neuroimaging. Neuron, 2020, 105, 600-603.	3.8	92

#	Article	IF	CITATIONS
55	Fusion in diffusion MRI for improved fibre orientation estimation: An application to the 3T and 7T data of the Human Connectome Project. NeuroImage, 2016, 134, 396-409.	2.1	91
56	High-Resolution Mapping of Myeloarchitecture In Vivo: Localization of Auditory Areas in the Human Brain. Cerebral Cortex, 2015, 25, 3394-3405.	1.6	90
57	Spatial organization of frequency preference and selectivity in the human inferior colliculus. Nature Communications, 2013, 4, 1386.	5.8	89
58	Reconstructing the spectrotemporal modulations of real-life sounds from fMRI response patterns. Proceedings of the National Academy of Sciences of the United States of America, 2017, 114, 4799-4804.	3.3	88
59	Feasibility of Using Ultra-High Field (7 T) MRI for Clinical Surgical Targeting. PLoS ONE, 2012, 7, e37328.	1.1	86
60	RASER: A new ultrafast magnetic resonance imaging method. Magnetic Resonance in Medicine, 2007, 58, 794-799.	1.9	85
61	The story of the initial dip in fMRI. NeuroImage, 2012, 62, 1103-1108.	2.1	85
62	High resolution data analysis strategies for mesoscale human functional MRI at 7 and 9.4 T. Neurolmage, 2018, 164, 48-58.	2.1	84
63	Study protocol: the Whitehall II imaging sub-study. BMC Psychiatry, 2014, 14, 159.	1.1	82
64	Functional mapping of the magnocellular and parvocellular subdivisions of human LGN. NeuroImage, 2014, 102, 358-369.	2.1	75
65	Processing of Natural Sounds: Characterization of Multipeak Spectral Tuning in Human Auditory Cortex. Journal of Neuroscience, 2013, 33, 11888-11898.	1.7	73
66	Sub-millimeter T2 weighted fMRI at 7 T: comparison of 3D-GRASE and 2D SE-EPI. Frontiers in Neuroscience, 2015, 9, 163.	1.4	70
67	Whole brain high-resolution functional imaging at ultra high magnetic fields: An application to the analysis of resting state networks. NeuroImage, 2011, 57, 1031-1044.	2.1	68
68	Lowering the thermal noise barrier in functional brain mapping with magnetic resonance imaging. Nature Communications, 2021, 12, 5181.	5.8	68
69	Neural correlates of visual form and visual spatial processing. Human Brain Mapping, 1999, 8, 60-71.	1.9	67
70	Further evaluation of the initial negative response in functional magnetic resonance imaging. Magnetic Resonance in Medicine, 1999, 41, 436-441.	1.9	64
71	Frontiers of brain mapping using MRI. Journal of Magnetic Resonance Imaging, 2006, 23, 945-957.	1.9	58
72	Simultaneous multi-slice Turbo-FLASH imaging with CAIPIRINHA for whole brain distortion-free pseudo-continuous arterial spin labeling at 3 and 7 T. NeuroImage, 2015, 113, 279-288.	2.1	57

#	Article	IF	CITATIONS
73	NOise reduction with DIstribution Corrected (NORDIC) PCA in dMRI with complex-valued parameter-free locally low-rank processing. NeuroImage, 2021, 226, 117539.	2.1	57
74	The nonhuman primate neuroimaging and neuroanatomy project. Neurolmage, 2021, 229, 117726.	2.1	57
75	Modeling and analysis of mechanisms underlying fMRI-based decoding of information conveyed in cortical columns. NeuroImage, 2011, 56, 627-642.	2.1	56
76	Processing of frequency and location in human subcortical auditory structures. Scientific Reports, 2015, 5, 17048.	1.6	54
77	Sensitivity and specificity considerations for fMRI encoding, decoding, and mapping of auditory cortex at ultra-high field. Neurolmage, 2018, 164, 18-31.	2.1	52
78	In vivo micro-MRI of intracortical neurovasculature. NeuroImage, 2006, 32, 62-69.	2.1	48
79	Retinotopic mapping with spin echo BOLD at 7T. Magnetic Resonance Imaging, 2010, 28, 1258-1269.	1.0	45
80	Microstructure Imaging of Crossing (MIX) White Matter Fibers from diffusion MRI. Scientific Reports, 2016, 6, 38927.	1.6	43
81	Magnetic Resonance Field Strength Effects on Diffusion Measures and Brain Connectivity Networks. Brain Connectivity, 2013, 3, 72-86.	0.8	42
82	High-Field fMRI for Human Applications: An Overview of Spatial Resolution and Signal Specificity. Open Neuroimaging Journal, 2011, 5, 74-89.	0.2	40
83	Spatial specificity of the functional MRI blood oxygenation response relative to neuronal activity. NeuroImage, 2018, 164, 32-47.	2.1	39
84	Linearity of blood-oxygenation-level dependent signal at microvasculature. NeuroImage, 2009, 48, 313-318.	2.1	38
85	Human habenula segmentation using myelin content. NeuroImage, 2016, 130, 145-156.	2.1	38
86	Strategies and prospects for cortical depth dependent T2 and T2* weighted BOLD fMRI studies. NeuroImage, 2019, 197, 668-676.	2.1	34
87	Processing complexity increases in superficial layers of human primary auditory cortex. Scientific Reports, 2019, 9, 5502.	1.6	32
88	Highâ€resolution wholeâ€brain diffusion MRI at 7T using radiofrequency parallel transmission. Magnetic Resonance in Medicine, 2018, 80, 1857-1870.	1.9	31
89	Characterizing cerebral hemodynamics across the adult lifespan with arterial spin labeling MRI data from the Human Connectome Project-Aging. NeuroImage, 2021, 230, 117807.	2.1	31
90	Variable flip angle 3Dâ€GRASE for high resolution fMRI at 7 tesla. Magnetic Resonance in Medicine, 2016, 76, 897-904.	1.9	30

#	Article	IF	CITATIONS
91	Ultra-high field (10.5 T) resting state fMRI in the macaque. NeuroImage, 2020, 223, 117349.	2.1	30
92	Decreases in ADC observed in tissue areas during activation in the cat visual cortex at 9.4 T using high diffusion sensitization. Magnetic Resonance Imaging, 2008, 26, 889-896.	1.0	29
93	Cortical fibers orientation mapping using in-vivo whole brain 7†T diffusion MRI. NeuroImage, 2018, 178, 104-118.	2.1	29
94	Featural and temporal attention selectively enhance task-appropriate representations in human primary visual cortex. Nature Communications, 2014, 5, 5643.	5.8	27
95	Multimodal 7T Imaging of Thalamic Nuclei for Preclinical Deep Brain Stimulation Applications. Frontiers in Neuroscience, 2016, 10, 264.	1.4	25
96	Recent Advances in High-Resolution MR Application and Its Implications for Neurovascular Coupling Research. Frontiers in Neuroenergetics, 2010, 2, 130.	5.3	23
97	Less noise, more activation: Multiband acquisition schemes for auditory functional MRI. Magnetic Resonance in Medicine, 2015, 74, 462-467.	1.9	23
98	Spin echo functional MRI in bilateral auditory cortices at 7T: An application of B1 shimming. NeuroImage, 2012, 63, 1313-1320.	2.1	22
99	Evaluating the Columnar Stability of Acoustic Processing in the Human Auditory Cortex. Journal of Neuroscience, 2018, 38, 7822-7832.	1.7	22
100	Human Connectome Project-style resting-state functional MRI at 7 Tesla using radiofrequency parallel transmission. Neurolmage, 2019, 184, 396-408.	2.1	22
101	Diffusion Imaging in the Post HCP Era. Journal of Magnetic Resonance Imaging, 2021, 54, 36-57.	1.9	22
102	Minimal specifications for non-human primate MRI: Challenges in standardizing and harmonizing data collection. NeuroImage, 2021, 236, 118082.	2.1	22
103	Toward next-generation primate neuroscience: A collaboration-based strategic plan for integrative neuroimaging. Neuron, 2022, 110, 16-20.	3.8	22
104	Pushing the spatio-temporal limits of MRI and fMRI. NeuroImage, 2018, 164, 1-3.	2.1	20
105	Empirical transmit field bias correction of T1w/T2w myelin maps. NeuroImage, 2022, 258, 119360.	2.1	20
106	A 3D wavelet fusion approach for the reconstruction of isotropicâ€resolution MR images from orthogonal anisotropicâ€resolution scans. Magnetic Resonance in Medicine, 2012, 67, 1167-1172.	1.9	19
107	Using precise word timing information improves decoding accuracy in a multiband-accelerated multimodal reading experiment. Cognitive Neuropsychology, 2016, 33, 265-275.	0.4	18
108	Using high spatial resolution fMRI to understand representation in the auditory network. Progress in Neurobiology, 2021, 207, 101887.	2.8	17

#	Article	IF	CITATIONS
109	In Vivo 7T MRI of the Non-Human Primate Brainstem. PLoS ONE, 2015, 10, e0127049.	1.1	17
110	Phaseâ€cycled simultaneous multislice balanced SSFP imaging with CAIPIRINHA for efficient banding reduction. Magnetic Resonance in Medicine, 2016, 76, 1764-1774.	1.9	16
111	An 8â€dipole transceive and 24â€loop receive array for nonâ€human primate head imaging at 10.5 T. NMR in Biomedicine, 2021, 34, e4472.	1.6	16
112	Estimation of the CSAâ€ODF using Bayesian compressed sensing of multiâ€shell HARDI. Magnetic Resonance in Medicine, 2014, 72, 1471-1485.	1.9	15
113	Functional MRI mapping neuronal inhibition and excitation at columnar level in human visual cortex. Experimental Brain Research, 2010, 204, 515-524.	0.7	14
114	Multiple Q-Shell ODF Reconstruction in Q-Ball Imaging. Lecture Notes in Computer Science, 2009, 12, 423-431.	1.0	14
115	Triple diffusion encoding MRI predicts intraâ€axonal and extraâ€axonal diffusion tensors in white matter. Magnetic Resonance in Medicine, 2020, 83, 2209-2220.	1.9	13
116	Representation of pitch chroma by multi-peak spectral tuning in human auditory cortex. NeuroImage, 2015, 106, 161-169.	2.1	12
117	New strategy for reconstructing partial-Fourier imaging data in functional MRI. Magnetic Resonance in Medicine, 2001, 46, 1045-1048.	1.9	11
118	Differential information content in staggered multiple shell hardi measured by the tensor distribution function. , 2011, , .		10
119	Temporal multivariate pattern analysis (tMVPA): A single trial approach exploring the temporal dynamics of the BOLD signal. Journal of Neuroscience Methods, 2018, 308, 74-87.	1.3	10
120	Multivoxel Pattern of Blood Oxygen Level Dependent Activity can be sensitive to stimulus specific fine scale responses. Scientific Reports, 2020, 10, 7565.	1.6	10
121	20-fold Accelerated 7T fMRI Using Referenceless Self-Supervised Deep Learning Reconstruction. , 2021, 2021, 3765-3769.		10
122	Spatial specificity of high-resolution, spin-echo BOLD, and CBF fMRI at 7 T. Magnetic Resonance in Medicine, 2004, 51, 646-647.	1.9	9
123	Clarifying the role of higher-level cortices in resolving perceptual ambiguity using ultra high field fMRI. NeuroImage, 2021, 227, 117654.	2.1	9
124	Filtering respiratory motion artifact from resting state fMRI data in infant and toddler populations. NeuroImage, 2022, 247, 118838.	2.1	9
125	High Magnetic Fields for Imaging Cerebral Morphology, Function, and Biochemistry. Biological Magnetic Resonance, 2006, , 285-342.	0.4	8
126	Nonadditive Two-Way ANOVA for Event-Related fMRI Data Analysis. NeuroImage, 2001, 14, 406-416.	2.1	7

#	Article	IF	CITATIONS
127	Ultra-high field (10.5T) diffusion-weighted MRI of the macaque brain. NeuroImage, 2022, 255, 119200.	2.1	7
128	Real-time motion monitoring improves functional MRI data quality in infants. Developmental Cognitive Neuroscience, 2022, 55, 101116.	1.9	7
129	Resting-state functional connectivity identifies individuals and predicts age in 8-to-26-month-olds. Developmental Cognitive Neuroscience, 2022, 56, 101123.	1.9	7
130	Statistical power or more precise insights into neuro-temporal dynamics? Assessing the benefits of rapid temporal sampling in fMRI. Progress in Neurobiology, 2021, 207, 102171.	2.8	6
131	Improved Simultaneous Multi-Slice Functional MRI Using Self-supervised Deep Learning. , 2021, , .		6
132	Design of a Robotic Stereotactic Device for Biopsy and Minimally Invasive Interventions in the Breast With Real Time MRI Guidance. , 2002, , .		2
133	The Use of Ultrahigh Field Functional MRI in Neuroscience Applications. , 2019, , 419-435.		1
134	Neural correlates of visual form and visual spatial processing. Human Brain Mapping, 1999, 8, 60-71.	1.9	1
135	Efficient estimation via envelope chain in magnetic resonance imagingâ€based studies. Scandinavian Journal of Statistics, 0, , .	0.9	0
136	How pushing the spatiotemporal resolution of fMRI can advance neuroscience. Progress in Neurobiology, 2021, 207, 102184.	2.8	0
137	Neuroscience applications of functional MRI. Advances in Magnetic Resonance Technology and Applications, 2021, , 261-276.	0.0	0